KSME International Journal, Vol. 15 No. 11, pp. 1599~1604, 2001

Vortex Ring, Shock-Vortex Interaction, and Morphological Transformation Behind a Finite Cone

Se-Myong Chang*
School of Mechanical and Aerospace Engineering, College of Engineering, Seoul National University, Seoul 151-742, Korea
Keun-Shik Chang
Department of Aerospace Engineering, Korea Advanced Institute of Science and Technology, Taejon 305-701, Korea

Axisymmetric compressible flow field induced by shock diffraction from a finite cone is investigated with experimental and computational methods. Double-exposure holographic interferograms show images of the density field integrated along the light path. Using the sight-integrated density based on the Able transformation, the axisymmetric computational results are compared qualitatively with the experiment. In the present paper, we observed some distinguishing flow physics: the fault structure of vortex ring, the shock-vortex interaction, and the morphological transformation of shock waves.

Key Words : Cone, Shock-Vortex Interaction, Axisymmetric Flow, Holographic Interferometry, Euler Equations

Nomenclature

c : Speed of sound
$erf(\eta)$: Error function $\left(=\frac{2}{\sqrt{\pi}}\int_{-\infty}^{\eta} e^{-\xi}d\xi\right)$
i, j : Indices of x and y direction
L : Length scale
M : Mach number
Re : Reynolds number
t^* : Nondimensional time scale $(=tU_\infty/L)$
x : Coordinate of symmetric axis
y : Coordinate of radial direction
γ : Specific heat ratio $(=1.4$ for air$)$
δ^* : Nondimensional thickness of boundary layer
ν : Diffusion coefficient $(=M_\infty/Re)$
θ_w : Semi-apex angle of a cone
$\bar{\rho}$: Sight-integrated density

Subscripts
s : Shock wave
∞ : Free stream value

* Corresponding Author,
E-mail : smc1972@dreamwiz.com
TEL : +82-2-880-1902; **FAX** : +82-2-887-2662
BK21 Assistant Professor, Aero-Acoustics and Noise Control Laboratory (301-1214), School of Mechanical and Aerospace Engineering, College of Engineering, Seoul National University, San 56-1 Silim-dong, Kwanak-gu, Seoul 151-742, Korea. (Manuscript **Received** May 17, 2001; **Revised** August 30, 2001)

1. Introduction

The study of conical shock diffraction has a long history because of its practical shape in ballistics. Bryson and Gross (1961) observed a strong shock diffraction in front of a cone, analyzing shock-shock interaction using the Whitham's theory. Recently, Han et al. (1992) obtained various relations on the Mach reflection from conical geometries. Yang et al. (1996) reported an experimental parametric study on the various shock Mach numbers and semi-apex angles, discussing the transition between von Neumann reflection and single Mach reflection.

Demarcated from the preceding literatures focussed on the front reflection of shock wave, in this paper a finite cone is used to produce a vortex ring and to induce a shock-vortex interaction.

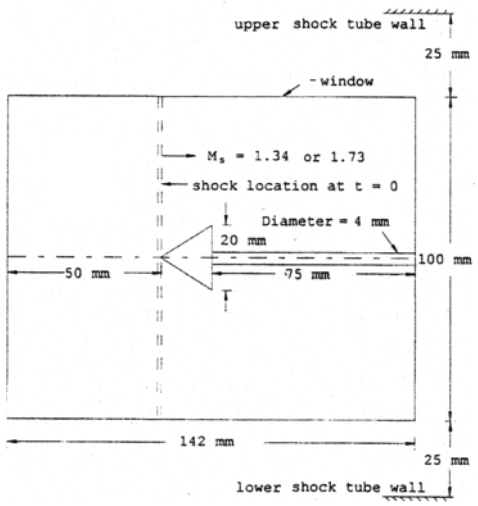

Fig. 1 Shock wave impinging into a finite cone

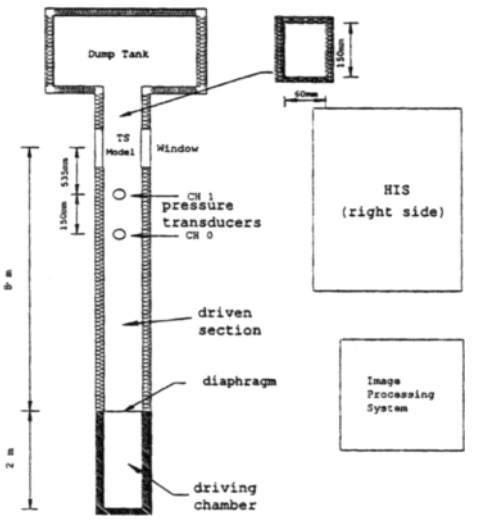

(a) KAIST shock tube

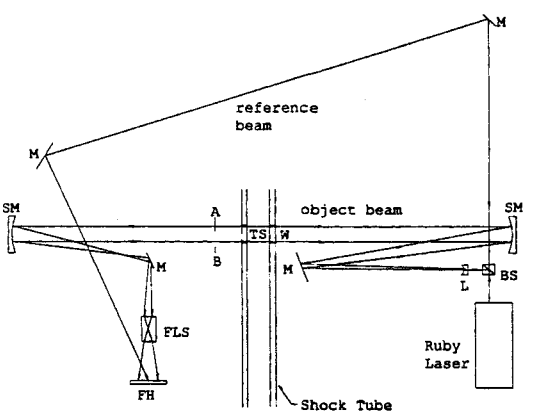

(b) HIS (Holographic Interferometry System)

Fig. 2 Experimental setup

This interaction shows a complicated but interesting feature in a contracted area. In Chang and Chang (2000), the present authors investigated shock-vortex interaction behind a truncated wedge, but the discussion was so restricted only to a two-dimensional problem and one shock Mach number, $M_s=1.34$. Now we extend our interest to an axisymmetric problem. The conceptual physics is visualized using the double-exposure holographic interferometry system installed in a shock tube. The flow field is also counter checked from the numerical solution of Euler equations on the quadrilateral unstructured adaptive grids.

2. Methods

2.1 Flow visualization

A finite cone of the equilateral triangular side view (20 mm) in Fig. 1 is installed in the KAIST shock tube, 60 mm × 150 mm cross section: see Fig. 2(a). The driver and test gases are all air at the standard atmospheric condition. The initial pressure at the test section is adjusted from 0.5 to 0.2 atm for a given shock Mach number. This model is supported by a circular stick of 4 mm diameter aligned to the symmetric axis. In the double-exposure holographic interferometry of Fig. 2(b), original images are stored on Agfa 8E75 sheet films taken by a 1 J ruby laser, and the developed holograms are reconstructed with 25 mW He-Ne laser.

Two representative incident shock Mach numbers are selected for this experiment: $M_s=1.34$ and $M_s=1.73$, measured and calibrated with two pressure transducers at the upstream position of test section, CH0 and CH1 in Fig. 2(a). For the two cases, the induced flow behind the incident shock is all subsonic. However, as commented in Sivier et al. (1992), locally supersonic regions can exist, and they are found in $M_s=1.73$ case due to strong motion of twin starting vortices, which will be discussed in Sec. 3.1.

2.2 Numerical analysis

The following is the Euler equations in the axisymmetric coordinate:

$$\frac{\partial}{\partial t}\begin{bmatrix}\rho\\ \rho u\\ \rho v\\ E\end{bmatrix}+\frac{\partial}{\partial x}\begin{bmatrix}\rho u\\ \rho u^2+p\\ \rho uv\\ (E+p)u\end{bmatrix}+\frac{\partial}{\partial y}\begin{bmatrix}\rho v\\ \rho uv\\ \rho v^2+p\\ (E+p)v\end{bmatrix}+\frac{1}{y}\begin{bmatrix}\rho v\\ \rho uv\\ \rho v^2\\ (E+p)v\end{bmatrix}=0 \quad (1)$$

where $p=(\gamma-1)[E-\rho(u^2+v^2)/2]$. Because the shock time scale (hundreds μs) is far less than the viscous time scale (hundreds ms), the inviscid assumption may be valid for this problem. From the dimensional analysis based on the Falkner-Skan flow and the Mangler transformation in Chang (2000), the boundary layer thickness developed from a cone is

$$\delta^* \sim \frac{\delta_{99\%}}{L}=\frac{3.220}{\sqrt{Re}}\sqrt{\frac{2}{m+1}} \quad (2)$$

where the boundary layer thickness is defined as 99% recovery of the free stream velocity, and m=1/15 for a $\theta_w=30°$ cone. The first-order approximate solution of the diffusion equation is

$$u(x,\ t)=f(\eta)=1-erf(\eta) \quad (3)$$

where

$$\eta=\frac{\delta^*}{\sqrt{4\nu t^*}}$$

See the derivation of Eq. (3) in Whitham (1974). The final result is $f(\eta)<0.0004$ if $\eta>2.521$ for one of our case, $M_\infty<0.45$, $Re=2.4\times10^5$, $U_\infty<$ 170 m/s, L=$10\sqrt{3}$ mm, and $M_s=1.34$. If we restrict the experimental time limit within 200 μs, the diffusion effect of viscosity is less than 0.1 % of that of steady state. It is just a rough approximation without considering the shear layer effect near the vortex, but gives us a conceptual guideline.

Equation. (1) is numerically integrated with a TVD (total variation diminishing) finite volume method on quadrilateral unstructured adaptive grids: see Sec. 3.2 of Chang and Chang (2001) in detail. Five levels of adaptive grids are used in the simulation.

2.3 Data treatment for axisymmetry

When the first and the second pulse beam transmit the media in the double-exposure holographic interferometry, the phase difference originated from the different light speed is recorded on the holographic films. The reference beam is later used for reconstruction of the object images. The light incident to an axisymmetric coordinate system has a sight-integrated effect along the propagating direction: see Mayinger (1994).

The sight-integrated density is expressed from the Able transformation as

$$\bar{\rho}(x,,\ y)=\frac{2}{\sqrt{R^2-y^2}}\int_{-y}^{R}\rho(x,\ \bar{y})\,d\sqrt{\bar{y}^2-y^2} \quad (4)$$

Eq. (4) for continuous data can be modified for discrete data:

$$\bar{\rho}_{i,j}=\frac{2\rho_{i,j}\sqrt{y_{j+1/2}^2-y_j^2}+\sum_{k=j+1}^{J}\rho_{i,k}a_{j,k}}{\sqrt{R^2-y_j^2}} \quad (5)$$

where

$a_{j,k}=2(\sqrt{y_{k+1/2}^2-y_j^2}-\sqrt{y_{k-1/2}^2-y_j^2})$ and $y_{J+1/2}=R$.

In this study, we obtained the field of sight-

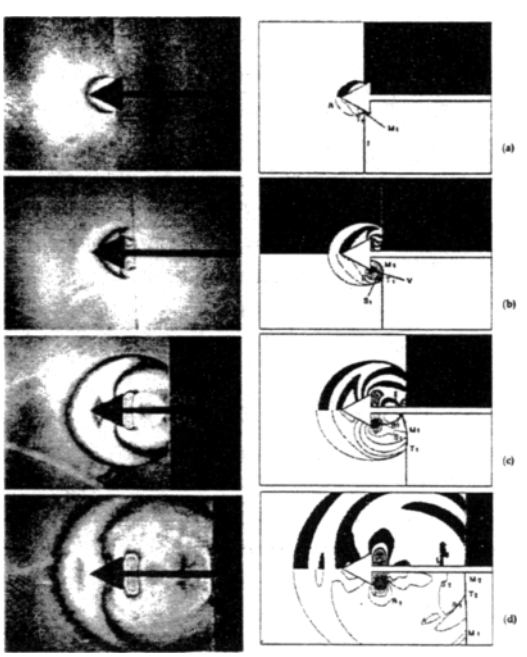

Fig. 3 Experimental interferogram (left), numerical isopycnics (right lower), and numerical interferogram (right upper), $M_s=1.34$. (a) 33μs; (b) 56μs; (c) 87μs; (d) 167μs

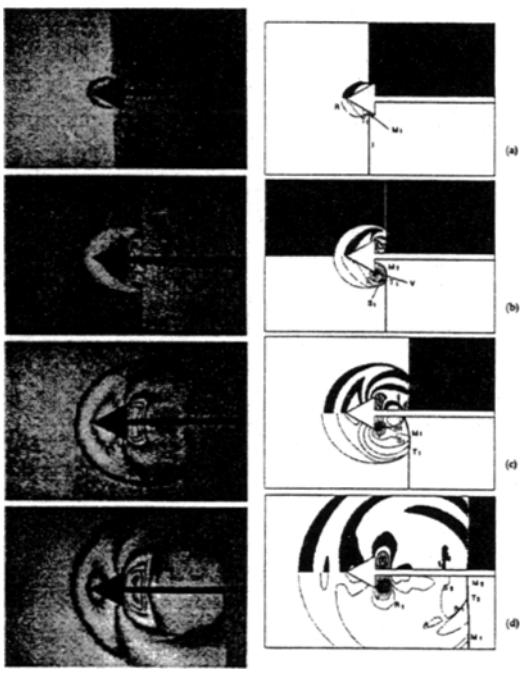

Fig. 4 Experimental interferogram (left), numerical isopycnics (lower right) and numerical interferogram (upper right), $M_s=1.73$. (a) 24μs ; (b) 38μs ; (c) 98μs ; (d) 139μs

integrated density $\bar{\rho}$, and produced numerical interferograms correspondent to experimental photographs by controlling $\Delta\bar{\rho}$ in the post processor. Strictly to say, the flow field is three dimensional since the shock tube has a rectangular cross section, and therefore the comparison between experiment and computation in Fig. 3(c)-(d) and Fig. 4(c)-(d) should be restricted to a qualitative one.

3. Flow Physics

The finite fluid elements can often generate a complex set of physics in gas dynamics. The basic elements are marked with capital letters in the related figures. To explain the physical phenomena, Fig. 3(a)-(d) and Fig. 4(a)-(d) are now considered one by one. In each frame, the left is an experimental interferogram (Sec. 2.1), the right lower is a computational isopycnics (Sec. 2.2), and the right upper is a numerical interferogram (Sec. 2.3).

The incident shock (I) collides with the cone, reflected in frame (a)'s, but the reflected shock (R) is far weaker than that of two-dimensional case. The single Mach reflection produces a tiny Mach stem (M_1) connected to the triple point (T_1). In frame (b)'s, the M_1 is diffracted at the sharp edge, causing the reversely running expansion fan (E). The vortex (V) originated at a vertex of the cone base collides with R_1, a reflection of M_1 to the symmetric axis in frame (c)'s. The shock-vortex interaction is not so remarkable in Fig. 3(d) or a weak interaction case, but the strong interaction case of Fig. 4(c)-(d) shows interactive elements, the waves A and D.

3.1 Vortex structure

The vortex (V) originated at the sharp vertex gradually grows to a vortex ring. The azimuthal velocity along a radial line parallel to the y axis and cutting the vortex center is plotted in Fig. 5 (a), which is obtained from the numerical result of Fig. 3(d) and Fig. 4(d). If we neglect the convective velocity, the speed $u(y)$ can be considered as the azimuthal velocity. The flow region is obviously divided into the rotational torus core and the outer irrotational flow. However, the saw-tooth shape faults are observed at the boundary between the two regions due to the Kelvin-Helmholtz instability.

It is obvious that there is locally supersonic regions for $M_s=1.73$ case whereas all regions are subsonic for $M_s=1.34$ case in Fig. 5(b). The maximum local flow Mach number increases upto $u/c=5.5$ at the slip layer ! Although such a high value is somewhat incredible since viscosity mitigates the flow pattern in actual situation, the existence of the strong supersonic region tells us the difference of flow regime between two cases.

3.2 Morphological transformation of shock waves

So far, the visualization of experiment shows a qualitative agreement with the Euler simulation. However, the delicate flow physics near the central axis is contaminated due to the sight integration effect. To investigate more deeply the dramatic wave physics, we make a supplementary

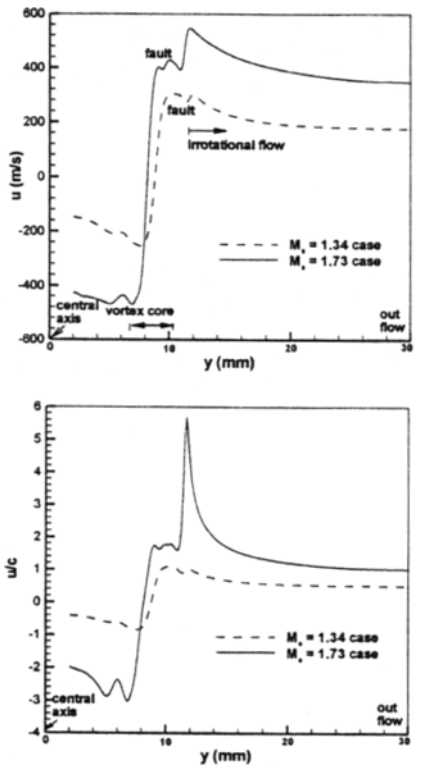

Fig. 5 Vortex structures : (a) azimuthal velocity profile, (b) local Mach number along a radial line

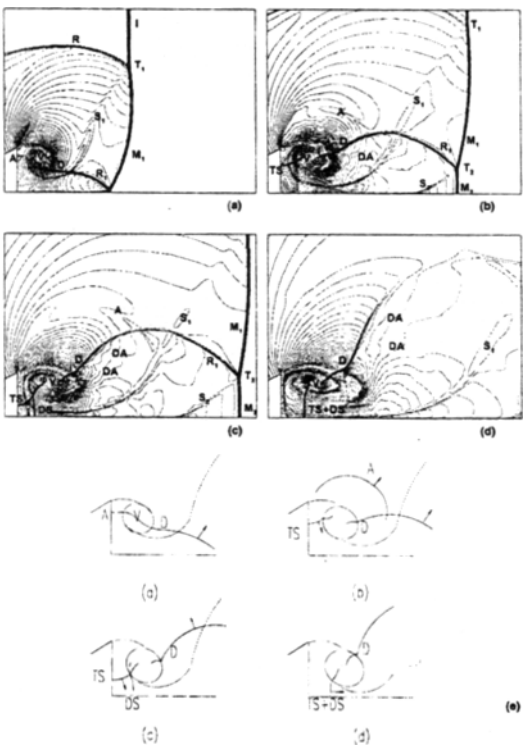

Fig. 6 Morphological transformation behind a finite cone, M_s=1.73 : numerical isopycnics (a) 63μs ; (b) 85μs ; (c) 98μs ; (d) 130μs ; (e) schematic

computation for the strong interaction case, M_s= 1.73.

The isopycnics for M_s=1.73 are provided in Fig. 6(a)-(d) to catch the instantaneous scenes of interaction between a shock (R_1) and a vortex (V). They are fundamentally equivalent to Fig. 4 (a)-(d), but differ in time counted from the first collision of the incident shock to the cone nose. R_1 is separated to the accelerated wave (A) near to cone base and the decelerated shock (D) caught by the vortex core of clockwise rotation in Fig. 6(a). The A escapes to outer flow while the tip of D named transmitted shock (TS) penetrates the vortex core in Fig. 6(b): this mechanism is explained in Chang and Chang (2000). Inside the entropy layer defined as the slip layer near the starting vortex (V) in Sivier et al. (1992), the shock (R_1) sweeps around the vortex edge producing diverging acoustics (DA). At the local compressive region behind the cone base, the reverse flow induced by the vortex (V) is steeply decelerated, making a new shock named decelerating shock (DS) in Fig. 6(c): refer to Fig. 1(c) of Hillier (1991), but the DS is soon caught and merged by TS in Figure 6(d). Finally, the morphological transformation from the shock R_1 to the shock $DS+TS$ is completed by the above mechanism. Fig. 6(e) is set of schematic diagrams for Fig. 6(a)-(d).

4. Conclusion

An axisymmetric shock diffraction behind a finite cone model for two kinds of flow regimes are studied with the holographic interferometry and the numerical solution of Euler equations. The vortex ring structure shows a slight fault at the boundary of vortex core and outer flow, and

local but steep supersonic flow regions are observed in the strong interaction case: see Fig. 5(a)-(b). Some phenomena different from those in the two-dimensional problem (Chang and Chang, 2000) are reported in this axisymmetric model. For example, in the strong interaction case, the transmitted shock (TS) and the flow-decelerating shock (DS) are merged to be morphologically transformed into a new shock ($TS+DS$), which is not yet made clear in the two-dimensional case: see Fig. 6(e).

References

Bryson A. E. and Gross R. F. W., 1961, "Diffraction of Strong Shocks by Cones, Cylinders, and Spheres," *Journal of Fluid Mechanics*, Vol. 10, pp. 1~16.

Chang S. M., 2000, "Unsteady Shock Wave -Vortex Interactions in the Compressible Shear Layer," Ph. D. Thesis of KAIST DAE965342.

Chang S. M. and Chang K. S., 1999, "Weak Shock Reflection from a Blunt Body," *Transaction of KSME (B)*, Vol. 23, pp. 901~910.

Chang S. M. and Chang K. S., 2000, "On the Shock-Vortex Interaction in Schardin's Problem," *Shock Waves*, Vol. 10, No. 5, pp. 333~343.

Chang S. M. and Chang K. S., 2000, "Visualization of Shock-Vortex Interaction Radiating Acoustic Waves," *Journal of Visualization*, Vol. 3, No. 3, pp. 221~228.

Chang S. M., Lee S. and Chang K. S., 2001, "Morphological Transformation of Shock Waves Behind a Flat Plate," *KSME International Journal*, Vol. 15, No. 5, pp. 676~682.

Han Z. Y., Milton B. E. and Takayama K., 1992, "The Mach Reflection Triple Point Locus for Internal and External Diffraction of a Moving Shock Wave," *Shock Waves*, Vol. 2, pp. 5~12.

Hillier R., 1991, "Computation of Shock Wave Diffraction at a Ninety Degree Convex Edge," *Shock Waves*, Vol. 1, pp. 135~144.

Mayinger F., 1994, "Fundamentals of Holography and Interferometry," In: Mayinger F (ed.) *Optical measurement - techniques and application*, Springer, pp. 27~50.

Sivier S., Loth E., Baum J. and Lohner R., 1992, "Vorticity Produced by Shock Wave Diffraction," *Shock Waves*, Vol. 2, pp. 31~41.

Whitham G. B., 1974, *Linear and Nonlinear Waves*, John Wiley, p. 33.

Yang J., Sasoh A. and Takayama K., 1996, "The Reflection of a Shock Wave over a Cone," *Shock Waves*, Vol. 6, pp. 167~273.